nature portfolio

https://doi.org/10.1038/s41558-022-01443-0

Supplementary information

Climate change threatens terrestrial water storage over the Tibetan Plateau

In the format provided by the authors and unedited

Supplementary Information for

Climate change threatens terrestrial water storage over the Tibetan Plateau

Xueying Li[1], Di Long[1]*, Bridget R. Scanlon[2], Michael E. Mann[3], Xingdong Li[1], Fuqiang Tian[1], Zhangli Sun[1], and Guangqian Wang[1]

1. State Key Laboratory of Hydroscience and Engineering, Department of Hydraulic Engineering, Tsinghua University, Beijing 100084, China

2. Bureau of Economic Geology, Jackson School of Geosciences, The University of Texas at Austin, Austin, TX 78758, USA

3. Department of Meteorology & Atmospheric Science, Penn State University, University Park, PA 16802, USA

*Corresponding author. Email: dlong@tsinghua.edu.cn

This PDF file includes:

Supplementary Text

1 TWS changes in individual basins over the GRACE period

For each TP basin, we first calculated TWS changes using top-down and bottom-up approaches during the GRACE period (2002–2017) and determined the most reliable GRACE solution over the TP. Top-down TWS changes were estimated from four GRACE solutions, i.e., CSR-M, JPL-M, CSR-SH, and JPL-SH. Bottom-up TWS changes were estimated by summing up water storage changes in glaciers, lakes, and subsurface components. These water storage changes were individually estimated using remote sensing (i.e., GRACE, satellite altimetry, and optical images) and LSMs (i.e., the latest LSMs including Noah and VIC in GLDAS-2.1 and CLSM in GLDAS-2.2). Summing up independent data sources could produce a reasonable range of uncertainties caused by inconsistencies among data sets, but bottom-up TWS changes provide a valuable reference for top-down satellite observations across the poorly gauged TP with complex climate systems (see Supplementary Section 4). In addition, we neglected some minor storage forms (e.g., snow, canopy, and reservoir water storage) in the bottom-up approach, because these components showed very small contributions to long-term trends in TWS relative to other components examined here (see Supplementary Section 4). Moreover, we did not specifically examine permafrost processes in the bottom-up components, because water storage changes caused by soil freezing/thawing could be reflected in changes in lake and/or subsurface storage through water transport [1].

We decomposed top-down TWSA time series into linear trends, interannual variability, seasonal amplitudes, and residual components. Considering the relatively short period of GRACE observations, we examined TWS trends in basins where linear trends contributed more than 50% of the total TWSA and coefficients of determination (R^2) of the fitted linear trends were higher than 0.49 (Fig.S4). TWS changes in these basins were dominated by linear trends rather than short-term variability. Related studies on long-term glacier variations in the Himalayas [2] and lake variations in the Inner TP [3] show significant glacier retreat and lake expansion since the 1990s, respectively. Such storage changes are generally consistent with those estimated during the GRACE period (see the following analysis). Moreover, we reconstructed TWS trends back to the 1980s using the developed ANNs (Fig.S5). The reconstructed trends in TWS for the past 40 years are generally consistent with those during the 2002–2017 period (Extended Data Fig.2), particularly across the basins where linear trends dominate total signals (e.g., the Indus, Ganges-Brahmaputra, Tarim, and Inner TP basins). These support the reliability of GRACE-based trend analysis across the TP basins with significant TWS changes, as opposed to short-term variability.

In addition to considering the contribution of linear trends to the total signal, we further selected basins with TWS trends $\geq$ 1 Gt/yr (Table S4) to explore trends in TWS and storage components. Overall, we compared top-down and bottom-up TWS changes and associated contributions from different components in the entire endorheic region, entire exorheic region, and seven TP basins including the Ganges-Brahmaputra, Indus, Inner TP, Salween-Mekong, and Tarim basins (Table S5). Based on climatic and geographic features, TWS changes over these seven TP basins were further grouped into three large regions for analysis: the Indus-Ganges-Brahmaputra (IGB) region featuring the largest maritime glacier concentration across the TP, the Salween-Mekong region featuring a wet and warm monsoon climate in the lower reaches, and the Tarim-Inner TP region that includes endorheic basins and is dominated by a continental climate. In addition, TWS variations over the Amu Darya basin are discussed individually, because it may emerge as a hotspot of water storage depletion in the future.

96% of the TP area shows significant trends with $p < 0.05$ based on the Mann-Kendall tests (Extended Data Fig.2). To estimate the contributions from glaciers, lakes, and subsurface water storage to TWS trends, we apportioned the percentages for each of the storage components scaled to match the top-down TWS changes estimated from JPL-M overall (Table S6). Neglecting minor storage forms (e.g., snow, canopy, and reservoir water storage) introduced slight uncertainties (see Supplementary Section 4). The IGB region showed a significant decrease in TWS of -13.2 Gt/yr ($p < 0.05$) where glacier retreat (-10.1 Gt/yr) accounted for ~76% of the depletion. Glaciers over this region store cold-season precipitation to compensate for warm-season water demand [4], which, together with snowmelt, supplies ~60% of total irrigation withdrawals in the Indus in the pre-monsoon period, impacting the livelihoods of ~130 million farmers on the Indo-Gangetic Plain [5]. Collapsing glaciers present great risk to local and downstream residents (e.g., debris from collapsing glaciers dammed the headwater of the Brahmaputra and threatened regions as far as Bangladesh with flooding in Oct 2018 [6]). Significant glacier retreat thus poses multiple threats to human settlements in the IGB region.

For the Salween-Mekong region, the top-down TWS observation also showed a decreasing trend (-3.2 Gt/yr; $p < 0.05$), with almost equal contributions from surface (-1.3 Gt/yr; accounting for ~42% of the depletion) and subsurface (-1.8 Gt/yr; accounting for ~58% of the depletion) storage changes. Surface water depletion was dominated by glacier retreat (-1.0 Gt/yr; accounting for ~33% of the TWS depletion), whereas subsurface depletion may be associated with intense degradation of seasonally frozen ground. Degradation of seasonally frozen ground may cause increases in subsurface runoff and soil evaporation, and thus translate to subsurface water storage declines. Spatial patterns of frozen soil over the TP and frozen soil degradation are shown in Fig.S6 and discussed by Zheng et al. [7]. Interpreting results for the Salween-Mekong region should be exercised with caution where the subsurface component contributed much to TWS changes, because subsurface trends may be underestimated by models relative to GRACE observations [8].

In contrast to exorheic basins, dominant contributors to TWS changes in the endorheic Tarim and Inner TP region differ between the two basins. TWS increased significantly (4.2 Gt/yr; $p < 0.05$) in the Inner TP where most TP lakes are situated (including ~300 TP lakes ≥ 10 km^2). We found that lake expansion (5.8 Gt/yr; $p < 0.05$) contributes ~137% but the subsurface component (-1.2 Gt/yr; $p < 0.05$) offsets ~30% of the total increasing trend. Although water resources in endorheic lakes are disconnected from downstream demand [9], extreme lake expansion may cause dikes to break and threaten the surrounding residents and railways (e.g., outbursts of Lake Kusai (35.73°N, 92.87°E) and Zhuonai (35.54°N, 91.93°E) in September 2011 in the Inner TP [10, 11]). Subsurface water storage declines may be related to large permafrost degradation in the Inner TP [7], similar to what is observed for the Salween-Mekong region. The Tarim basin has largely distributed glaciers from the Karakoram and Western Kun Lun Mountains and we found that glacier mass gain (0.9 Gt/yr), contrasting with glacier mass loss in the rest of the TP [12, 13], dominates TWS changes (1.1 Gt/yr; $p < 0.05$) across this basin (accounting for ~80% of the TWS increase).

The endorheic Amu Darya basin mainly showed seasonal variations in TWS with a slightly decreasing trend (-0.7 Gt/yr; $p < 0.05$). The negative glacier mass balance (-0.6 Gt/yr; accounting for ~88% of TWS change) is also a key determinant to TWS depletion, whereas the rate of glacier mass loss is lower than that in the exorheic IGB region. Different from the endorheic Inner TP basin that is disconnected from downstream water use, solid water resources stored in glaciers and snowpack are highly important for downstream irrigation in the Amu Darya basin [14]. Despite the slight glacier mass loss during the past 2002–2017 period, water storage changes in the Amu Darya basin require much attention because the stability of this water tower in the future could significantly impact downstream water availability.

2 Impacts of climate drivers on historical TWS changes

With little human disturbance in the high-mountain region, TWS variations over the TP are explained mostly by climate change. Here we considered climate impacts on TWS changes from changes in monsoon-dominated precipitation and warming-induced precipitation phase, and different roles in temperature rising and surface shortwave radiation across the TP from the perspectives of seasonal and spatial patterns. In general, precipitation is the major contributor to increased TWS, as it can result in glacier mass gain, lake expansion, and can augment soil moisture and groundwater storage. High temperature and surface shortwave radiation can lead to accelerated glacier melt and increased ET, which are the dominant causes of TWS declines. We realize that impacts of other factors, such as ET [15], morphology [16], and the glacier state of debris cover [12] are difficult to isolate for certain local studies, but this work provides an enhanced understanding of competing effects of three critical climate forcing (i.e., precipitation, temperature, and surface shortwave radiation) across the entire TP. In addition, TWS changes can be calculated by the difference between hydrologic input and output fluxes, i.e., precipitation minus ET and runoff, from a water-balance perspective. However, it is difficult to derive robust relationships between changes in TWS and hydrologic fluxes over the TP basins, due to the one-to-many responses and high interdependence among these variables, and large uncertainties in estimating ET and runoff fluxes. Relationships between changes in TWS and water balance components are shown in Supplementary Section 5.

We present climate impacts from precipitation, temperature, and surface shortwave radiation on TWS changes in both regionally averaged (Fig.S7) and spatially explicit patterns (Extended Data Fig.5) to show more detailed mechanisms. Trends in basin-averaged climate factors may not be statistically significant due to large spatial variability across the TP (see p values shown below in this section). However, we find significant trends in some critical areas that are strongly associated with TWS changes (Extended Data Fig.5). For instance, significant decreases in precipitation occurred in the Himalayan region of the Brahmaputra basin, significant increases in temperature occurred in the lower reaches of the Salween-Mekong region, and significant decreases in surface shortwave radiation occurred in the West Kunlun Mountains of the Tarim basin.

Significant TWS declines over the exorheic IGB region during the GRACE period (2002–2017) arise mostly from glacier retreat, which may be jointly explained by decreases in precipitation due to the recent weakening of the South Asia Summer Monsoon (SASM) and rising temperatures especially in winter. Several indices of the SASM including the Indian Summer Monsoon Index (IM Index) [17] and Webster and Yang Monsoon Index (WYM Index) [18], show a decline during the 1948–2019 period, with an acceleration during the past two decades (Fig.S8). Defining an integrative monsoon index (IMI) applied to both historical (CMIP3) simulations and NCEP-NCAR observations, Fan et al. [19] found a clear decreasing trend in both observations and historical simulations, though the simulations are seen to underestimate the magnitude of the observed decrease.

A weakening of the SASM reduces water vapor transport from the Indian Ocean to the TP leading to potential decreases in monsoonal precipitation over the monsoon-dominated Himalayan region, though this trend is at least partially offset by increased water vapor mixing ratios due to warming [19]. Annual precipitation across the Ganges-Brahmaputra basins decreased at a rate of -4.5 mm/yr ($p > 0.05$) during the 2002–2017 period based on multisource remote sensing observations [20] and, particularly, summer precipitation (June–August) decreased at a rate of -3.8 mm/yr ($p > 0.05$) that dominated annual precipitation variability. Decreases in annual and summer precipitation in the Ganges-Brahmaputra region reduced glacier accumulation in summer and could be one important reason for TWS declines. In addition, we find a significant warming trend in the Brahmaputra basin at a rate of 0.05 °C/yr ($p < 0.05$) based on ERA5 reanalysis data [21], and particularly in winter (at a rate of 0.07 °C/yr ($p > 0.05$)). This warming trend could accelerate glacier melt and snow sublimation and thus translate into TWS declines. For the Indus basin, although it is less affected by the South Asia monsoon and annual precipitation shows little change, we find decreases in winter precipitation (December–February) (-0.6 mm/yr ($p > 0.05$)). This appears to cause reduced glacier accumulation in winter. Both summer and winter temperatures in the Indus basin show little change, meaning that changing temperatures play a minor role in TWS variations here for the 2002–2017 period. Salween-Mekong has undergone significant decreases in TWS caused by depletion in glacier and subsurface water storage. A warming trend with annual average temperatures at a rate of 0.05 °C/yr ($p > 0.05$) may largely drive TWS changes over the Salween-Mekong region, resulting in not only the negative glacier mass balance, but also depletion in subsurface water storage related to degradation of seasonally frozen ground.

For the endorheic Tarim-Inner TP region, the climatic mechanisms underlying TWS changes are more complicated. Glaciers showed opposite trends in the Tarim basin where the observed glacier mass gain dominated increases in TWS, contrasting with the rest of TP glaciers which showed mass loss. Despite a warming trend over the Tarim basin (0.05 °C/yr ($p > 0.05$)), rising temperatures played less of a role, because both field-based [22] and model-based [23] studies indicate that shortwave radiation was more important in driving glacier melt over this region. We examined the trend in surface shortwave radiation from ERA5 reanalysis data [21], and found that annual and summer surface shortwave radiation decreased at a rate of -6.1 ($p > 0.05$) and -5.1 ($p > 0.05$) $MJ/m^2/yr$, respectively. The decreasing trend in surface shortwave radiation in the Tarim basin, particularly across the Karakoram and Western Kun Lun Mountains, is consistent with increased cloudiness as previous studies show [12, 24]. Because shortwave radiation could partly explain surface energy input for glacier melt, such a decrease may result in a positive mass balance. In the Inner TP with a concentrated lake distribution, annual precipitation features an increasing trend in the north but a decreasing trend in the south. This is generally consistent with the spatial pattern of TWS changes (Extended Data Fig.2), meaning that changes in precipitation are critical to TWS over this region. In addition, rising temperatures at a rate of 0.06 °C/yr ($p < 0.05$) may be linked to permafrost degradation and further result in depletion in subsurface water storage in the Inner TP.

In the Amu Darya basin, both annual precipitation and average temperature remain almost stable. Stable temperatures protect glaciers here from rapid retreat relative to what happened in the IGB region. A decreasing trend in winter precipitation (-0.7 mm/yr; $p > 0.05$), particularly on the Pamirs (Extended Data Fig.5 (g)) could have reduced glacier accumulation and led to slight TWS declines. In addition to the basin-averaged analysis, spatial patterns of trends in climate factors showed stronger linkages between climate and TWS changes.

Another important influence on TWS changes is warming-induced changes in precipitation phase, particularly over glacierized regions. The ratio of snowfall to total precipitation, estimated from the Global Precipitation Measurement (GPM) mission, decreased in both summer and winter months during 2002–2017 over the Indus, Ganges-Brahmaputra, and Amu Darya basins (Fig.S9 (a)–(c)). In the Indus, Ganges-Brahmaputra, and Amu Darya basins that showed negative glacier mass balances, summer snowfall ratios decreased by 17% (from 0.143 to 0.118), 26% (from 0.125 to 0.092), and 24% (from 0.152 to 0.116) from 2002 to 2017, respectively. In contrast, winter snowfall ratios decreased by 4% (from 0.871 to 0.838), 2% (from 0.824 to 0.808), and 3% (from 0.847 to 0.826), respectively. As for the Tarim basin that showed glacier mass gain, the summer snowfall ratio slightly decreased from 0.051 to 0.039, whereas the winter snowfall ratio remained stable (Fig.S9 (d)). A warming-induced change in precipitation phase from snowfall to rainfall is thus a factor influencing glacier mass changes over the TP. The glacier mass balances in the Indus, Ganges-Brahmaputra, and Amu Darya basins are affected by less snowfall, while snowfall ratios in the Tarim basin could have a minor impact.

3 Advantages of machine-learning TWS projection in this study

Reconstruction and projection of TWS changes over high-mountain regions is challenging for both data-driven and modeling approaches. To validate advantages of the improved machine learning method used here, we examined results of TWS projection from global hydrologic models and one previous machine learning study. As for model simulated TWS, we extracted outputs over the TP of 23 models that are available from the ISIMIP portal, including five hydrologic models and one dynamic vegetation model that are forced by four climate models (Table S8). We then calculated storage anomalies relative to the 2004–2009 time-mean baseline. Compared to GRACE observations, model-based TWSA shows neither trends nor spatial differences during the historical 2002–2017 period. In addition, during the projection period (2021–2060), different models have large uncertainties and the ensemble mean TWSA could only show seasonal variations without any trends (Fig.S10). These results indicate that these hydrologic models largely underestimate trends in TWSA [8], particularly over high-mountain regions with complex atmospheric circulation, terrain, and cryospheric processes. Therefore, we used a data-driven method to reconstruct and project TWSA over the TP rather than relied on model simulations.

However, previous studies on use of machine learning to reconstruct TWS changes were not applicable to the TP because of the complex relationship between TWS and climate forcing variables in glacierized regions. Sun et al. [25] used three machine learning approaches in GRACE reconstruction for grid cells and 60 basins globally. The input layer of machine learning models in Sun et al. [25] included monthly precipitation, temperature, and model simulated soil moisture storage. We examined the reconstructed results over the TP, IGB, Salween-Mekong, Amu Darya, and Tarim-Inner TP regions, and found that the reconstructed TWSA from the above study failed to detect significant increasing (e.g., the Tarim-Inner TP region) or decreasing (e.g., the IGB region) trends in TWS (Fig. S11). In addition, reconstructed TWSA during the gap period (Jul 2017–May 2018) was not consistent with GRACE and GRACE-FO observations.

Therefore, we improved the input layer of ANN models based on the water balance (Input fluxes – Output fluxes = TWS changes), and incorporated accumulated flux variables (i.e., accumulated precipitation and surface shortwave radiation) and state variables (i.e., air temperature and modelled TWS) to build non-linear relationships between predictors and GRACE TWSA (see Methods; Fig.S12). Given climatic mechanisms on historical TWS changes, precipitation should be the major input for TWS mass gain, whereas temperature and radiation are two proxies that could cause TWS loss. In addition, we incorporated the latest model projected TWS that could add more information on the physical process. Although machine learning models do not explicitly isolate physical processes, hydrologic principles could be used to guide selection of predictors. The water balance principle used in this study is similar to Mo et al. [26] that used accumulated inflow and outflow fluxes, and state variables (i.e., temperature and model simulated TWS) as the input layer. Moreover, accumulated flux variables were evaluated to be strongly linked with storage changes over the TP, e.g., Zhang et al. [27] demonstrated that accumulated standardized precipitation showed stronger linkages with lake mass changes (a cumulative basin-wide water gain) than monthly precipitation.

Projections from the improved ANN models in this study outperformed TWSA reconstructions from both hydrologic models and the previous machine learning study [25] mentioned above. ANN outputs in the testing sets (~15% samples) show good performance, with mean and median *KGE* values from TP grid-cells exceeding 0.9 for reconstructed TWSA from all CMIP6 forcings (Fig.S13). The reconstructed TWSA could successfully capture spatial patterns (Fig.3 (a)) and trends in time series (Fig.S14), and show reasonable uncertainty ranges during the gap period of GRACE and GRACE-FO (Jul 2017–May 2018). In particular, we used the latest GRACE-FO observations during Jun 2020–Aug 2021 that were excluded from training, validating, and testing ANN models, to perform further validation for the TWSA projection (Fig.S14). The projected TWSA in five regions (the TP, IGB, Salween-Mekong, Amu Darya and Tarim-Inner TP regions) showed good agreement with observations in both magnitude and trend, indicating the reliability of the improved ANN models for predicting TWSA in the future.

To further examine the improved machine learning models, we checked both bias and normalized root mean square error of ANN outputs in the testing sets from each grid cell, and found good performance (approaching zero) for both indices from all CMIP6 forcings (Fig.S15). This could support that the ANN models successfully captured the relationships between the input predictors and target variable rather than overfitting, because an overfitted model is generally known to have low bias but high variance. Moreover, error distribution curves are close to the normal distribution for ANNs with different forcing models (Fig.S16), indicating the randomly distributed model error and low risk of overfitting.

In addition, major conclusions of the projected TWSA in this study could be corroborated by physically based glacier projection [28]. For example, our machine learning-projected TWS changes show that the magnitude of TWS changes could be greatly reduced by the mid-21st century (particularly during the 2031–2060 period) after significant TWS changes over the past two decades (Fig.3 (a) and (c)). This conclusion is supported by separate projections of glacier mass balance [28], indicating that glacier melt in major river basins on the TP (e.g., Brahmaputra and Ganges) peaks over the next two decades followed by a decrease. Our study indicates that increases in precipitation by the mid-21st century would slow down significant TWS declines over the Ganges-Brahmaputra region. However, in the Amu Darya and Indus basins without large increases in precipitation, long-term climate change could lead to severe water loss under a warming future. This conclusion is partly supported by Rounce et al. [28], showing that the Eastern Himalayas (the Brahmaputra basin) is projected to experience less relative mass loss than other regions due partly to increases in precipitation but less increase in temperature. But the Pamir-Alay (the Amu Darya basin) may have severe mass loss as it gets warmer but not wetter. Overall, through comparisons with related studies and independent validation, the TWSA projection of this study could be reliable.

4 Sources of uncertainty in the bottom-up approach

Sources of uncertainty in the bottom-up approach mainly include inconsistencies and different spatial resolutions among various data sets, uncertainty from each component estimation, and the neglect of some forms of water storage. Storage changes in this study were independently estimated from optical satellite stereo pairs (glacier storage), satellite altimetry (lake storage), and LSMs (subsurface water storage), respectively. Remote sensing-based surface component estimation can be regarded as direct observations that were built on well-developed methods. Subsurface components were estimated from the mean subsurface water storage estimates from three GLDAS LSMs, where soil moisture and groundwater storages were not explicitly distinguished for certain layers.

Inconsistencies among three LSMs exist because these models rely on different sources of forcings and have different vertical levels for subsurface simulation. Both NOAH and VIC models only simulate soil moisture storage without considering groundwater storage. NOAH has explicit four layers for soil depths (0–10, 10–40, 40–100, 100–200 cm), whereas VIC has three soil layers with spatially varied depths. CLSM does not have explicit vertical levels for soil moisture. Instead, soil moisture is represented in surface (0–2 cm), root zone (0–100 cm), and profile (varies grid-by-grid) reservoirs. With data assimilation from GRACE (GRACE-DA) [29], the CLSM model does simulate shallow groundwater. In addition, all three LSMs consider the frozen soil process in the simulation [30, 31, 32], which could partly represent the permafrost process over the TP. However, systematic inconsistency could be reduced because we calculated subsurface storage anomalies for each model before deriving the averaged trend to compare with other data sources. Despite uncertainty in not explicitly distinguishing soil and groundwater components, this could be a reasonable proxy for subsurface storage, due to the lack of observations or satellite-based estimation. In the bottom-up approach, summing up independent data sources with different spatial resolutions should produce minor uncertainties, because we compared bottom-up and top-down TWS changes at the basin scale, as opposed to a grid cell scale (or a pixel scale).

Uncertainties in estimating changes in each water storage could affect the reliability of the TWS reference derived from the bottom-up approach. Well-developed methods were used in estimating surface storages to reduce uncertainty. For example, data sets from Brun et al. [33] are generated from the vast amount of freely available ASTER optical satellite stereo pairs to reveal more spatial details with a resolution of 30 m×30 m. Li et al. [34] proposed optical water levels based on regression relationships between lake shoreline changes and altimetry-based water level variations, to largely remove the systematic bias in combining multiple altimetric missions. Through field experiments and rigorous theoretical verification, uncertainties in glacier and lake storage changes were estimated to be ±20% [33] and ±6% [34] for the entire TP, respectively. This could be considered among the arguably best dataset to well reflect surface storage changes. Because surface components dominate TWS changes for most of TP basins except the Salween-Mekong region, we think that the bottom-up derived TWS changes could provide a benchmark to compare with GRACE TWS changes. As for the subsurface component, we acknowledge that GLDAS models have inherent limitations for underestimating storage trends [8]. However, ensemble mean of the three LSMs could partly reduce uncertainty and be a reasonable proxy.

Another uncertainty source for bottom-up derived TWS changes is the neglect of some water storage (e.g., snow, canopy, and reservoir water storage). This could also lead to the difference between TWS estimated from the bottom-up and top-down approaches, because GRACE-based top-down TWS changes include water storage of all forms. However, the neglected water storages (e.g., snow, canopy, and reservoir water storage) show very small long-term trends over this region. For example, snow water equivalent shows < 0.1 Gt/yr changes across TP basins (Fig.S17). The number of reservoirs on the vast TP is extremely limited (28 reservoirs in total with a total surface water extent of 1,248 km^2 (relative to an area of ~ 3 million km^2 for the entire TP)) (Fig.S18) and most of the existing reservoirs are regulated annually. This would not result in large trends over the past two decades. Therefore, it is reasonable to consider contributions from the major surface water components including glaciers and lakes, and subsurface components.

5 Relationships between changes in TWS and water balance components

We explored mechanisms underlying TWS changes from changes in climate variables (precipitation, temperature, and surface shortwave radiation) that influence the water-energy exchange of the hydrologic system and further drive TWS changes. From another perspective of water balance, TWS changes can be calculated by the difference between hydrologic input and output fluxes, i.e., precipitation minus ET and runoff. However, it is difficult to derive robust relationships between changes in TWS and hydrologic fluxes over the TP basins, due to the one-to-many responses and high interdependence among these variables, and large uncertainties in estimating hydrologic fluxes.

First, TWS changes are the integrated response to changes in precipitation, ET, and runoff. As the major water input, precipitation could largely impact both flux and storage variables in the water cycle, but distinguishing the impacts from ET and runoff on TWS changes may be ineffective. ET is related to both precipitation and energy limitation (radiation), and we find slight trends in long-term ET (Fig.S19 (a)). Basin runoff is strongly correlated with precipitation (Fig.S19 (b)–(d) as an example), and the timing and magnitude of runoff is also impacted by storage changes, e.g., glacier mass loss-induced meltwater. Therefore, except precipitation, the other two flux variables (ET and runoff) are not fundamental drivers of TWS changes. Instead, they both are dependent on other climate drivers (precipitation and radiation), and interact with TWS changes.

Second, reliable ET estimation over the TP could be a major challenge due to the complex high-mountain terrain [35, 36]. Current ET products (both remote sensing retrievals and model simulations) show large differences over the TP basins. Therefore, it would be more accurate to use precipitation, gauge-observed runoff and GRACE-derived TWS changes to infer ET based on the water balance equation [37]. Due to advances in remote sensing for estimating storage changes, reliable streamflow measurements at gauging stations, and more precipitation gauges than ET flux towers, ET estimation may have the largest uncertainty among the hydrologic components in the water balance. As for runoff estimation, despite its accuracy, runoff observations are limited in poorly-gauged TP basins. Therefore, ET and runoff fluxes are subject to low accuracy and limited coverage, which may not be appropriate for analyzing their relationships with TWS changes.

Overall, the fundamental drivers for TWS changes are climate forcing. Hydrologic fluxes in the water balance are interdependent, but it is difficult to distinguish the role of each component. Moreover, considering large uncertainty in ET and limited runoff observations over the TP, we analyzed climate mechanisms underlying TWS changes from the impacts of precipitation, temperature, and surface shortwave radiation.

Supplementary Figures

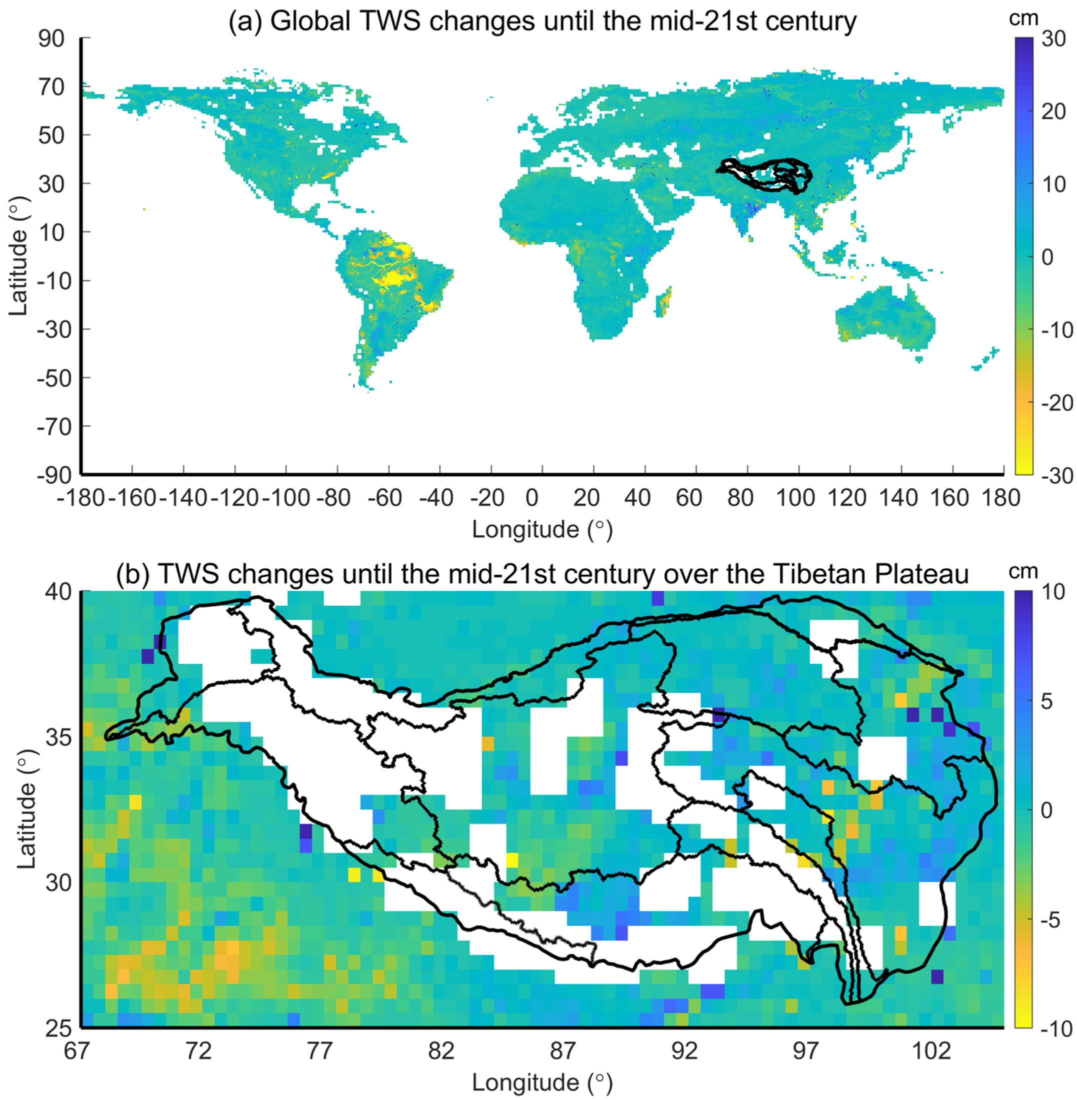

Fig. S1 Absence of TWS projections over the Tibetan Plateau from the literature. Data for generating this figure were provided by Pokhrel et al. [38], which linked projected future drought changes to TWS at the global scale. Changes were calculated by the difference between the average for the 2030–2059 period relative to the average for the 1976–2005 under the mid-range forcing scenario (RCP6.0) at the **(a)** global and **(b)** Tibetan Plateau scales.

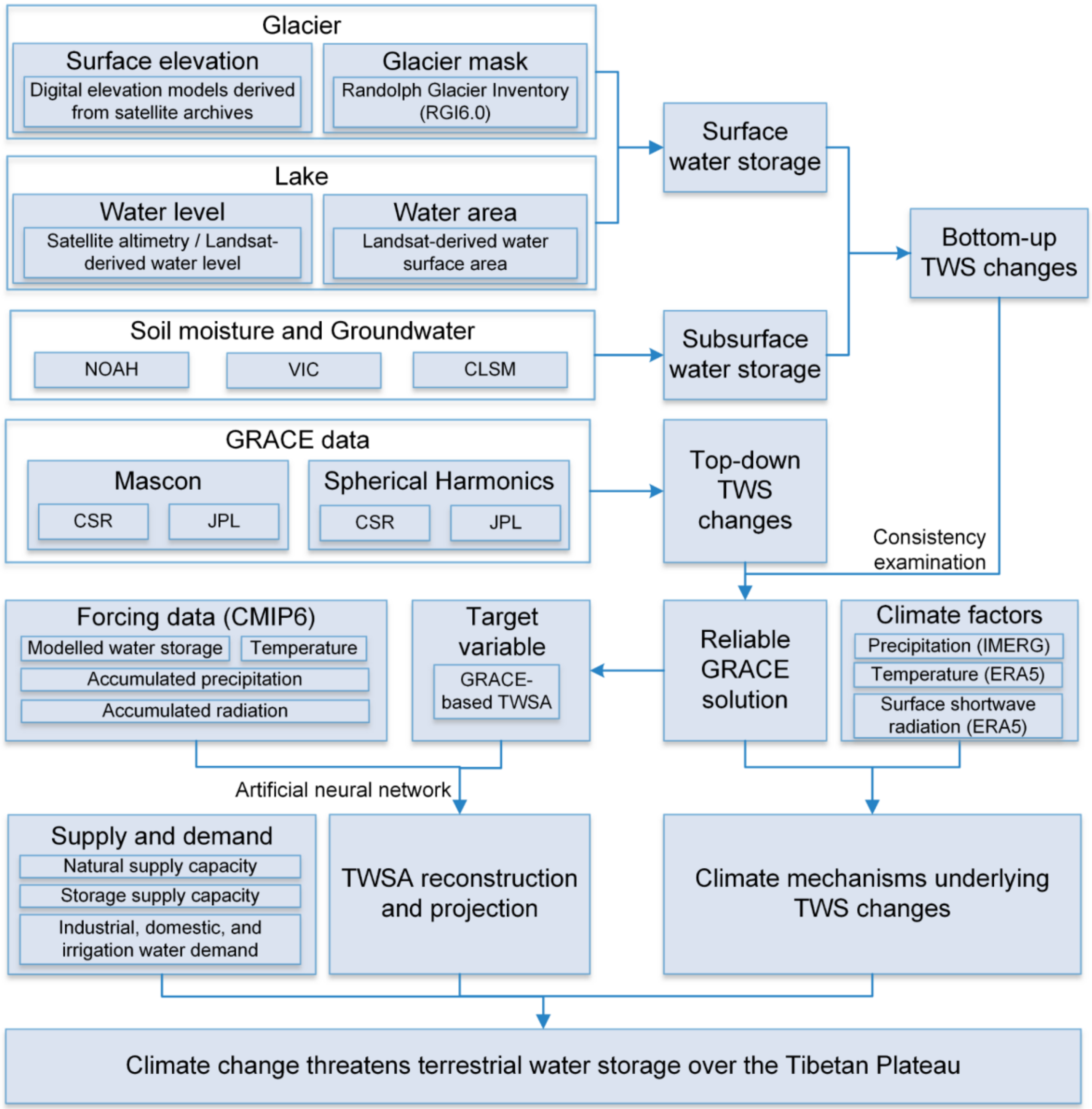

Fig. S2 Flowchart of this study. Analysis includes consistency examination between TWS changes estimated from the bottom-up and top-down approaches, assessing climate mechanisms underlying water storage changes, predicting TWS changes in the future, and quantifying impacts of TWS changes on water supply and demand.

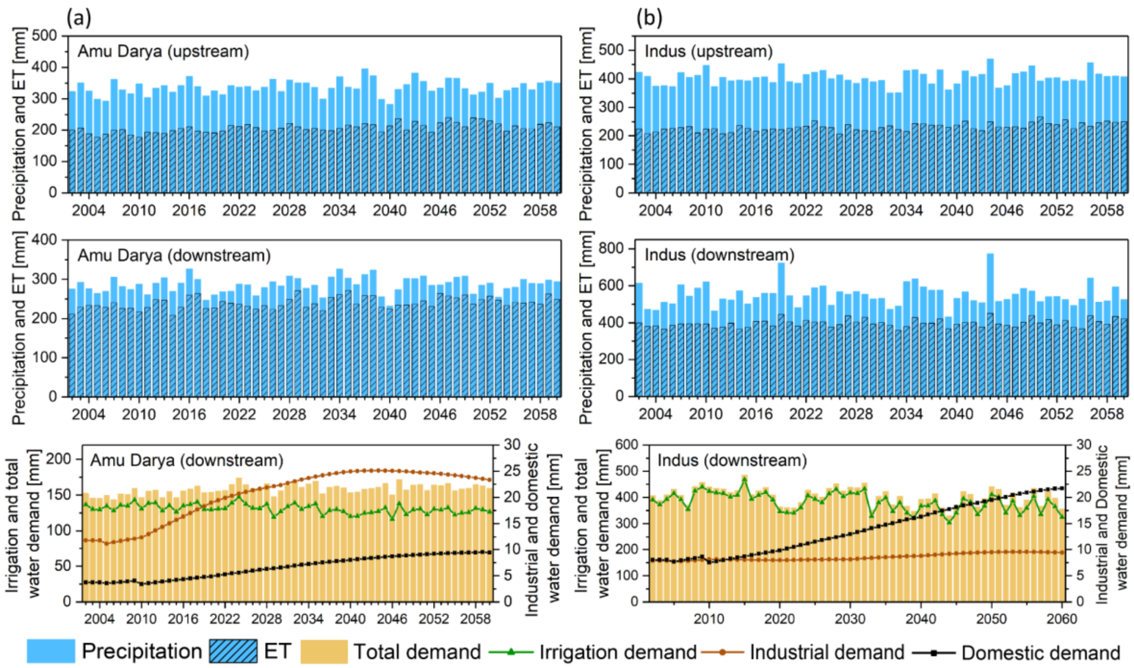

Fig. S3 Variations in precipitation, ET, and water demand during 2002–2060. Basin-averaged annual estimates are presented in the **(a)** Amu Darya and **(b)** Indus basins. Both precipitation and ET were the ensemble mean of nine global climate models and bias-corrected (see Methods). Total water demand includes irrigation, industrial, and domestic water demand. Irrigation water demand was estimated from actual irrigation withdrawal of the LPJml model. Industrial and domestic water demands were provided by the International Institute for Applied Systems Analysis.

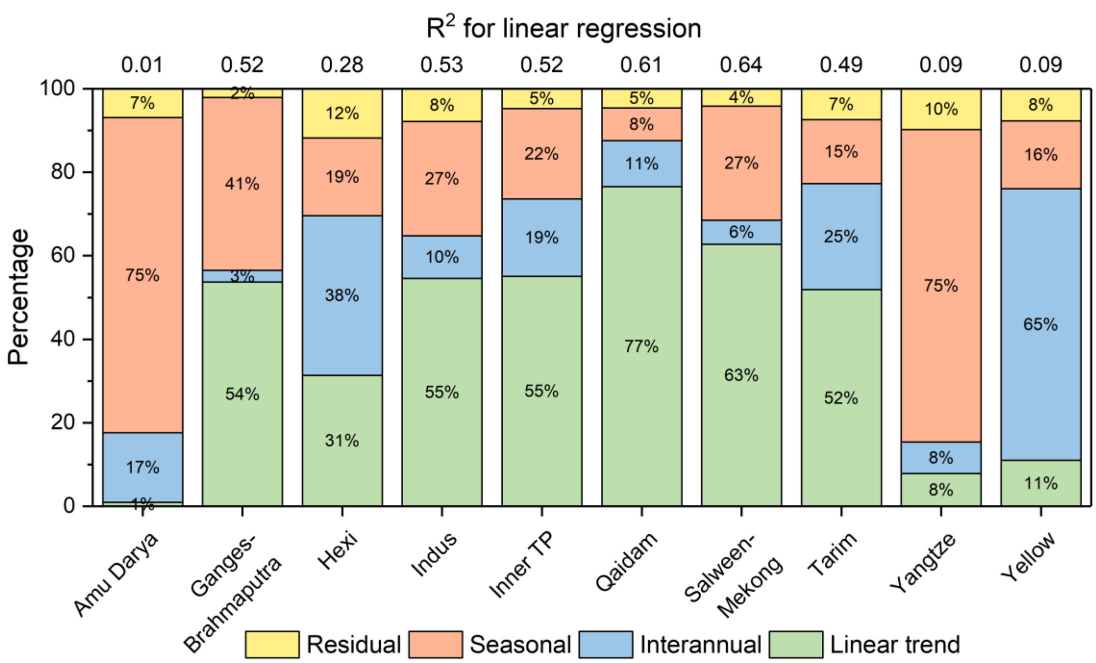

Fig. S4 Contributions of temporal components to the GRACE signal. Temporal components include the linear trend, interannual variability, seasonal amplitudes, and residual, which were estimated by the STL decomposition of GRACE JPL-M. The coefficient of determination (R^2) for the linear trend relative to the total signal of TWSA is also shown.

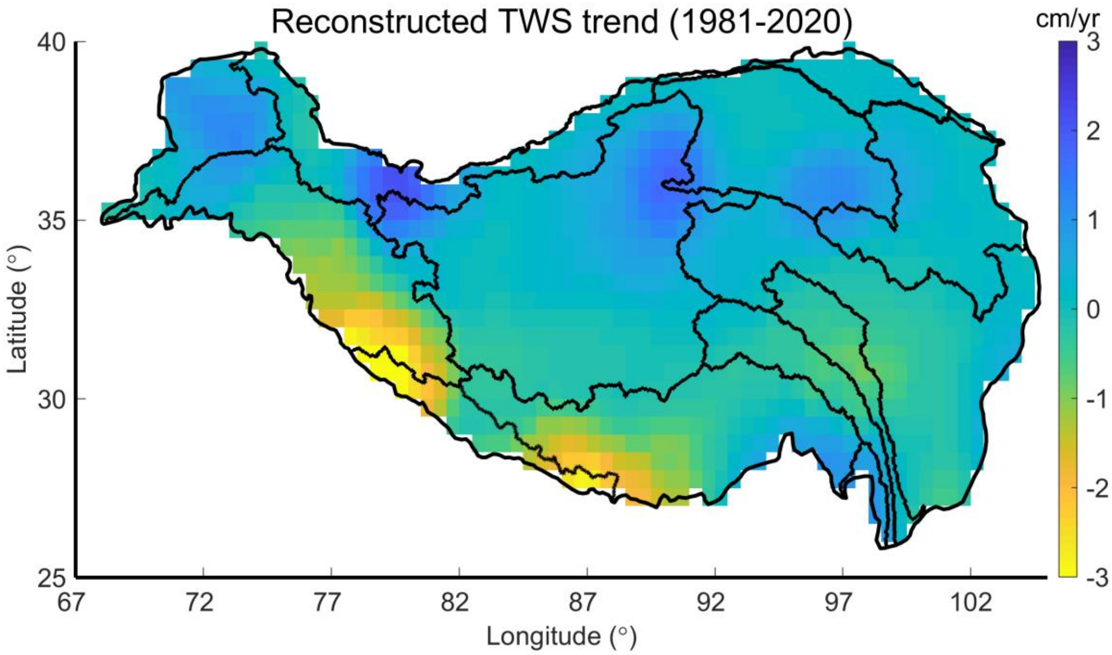

Fig. S5 Reconstructed TWS trends over the Tibetan Plateau during 1981–2020 using machine learning. The input layer for the backward reconstruction includes forcing data derived from ERA5 (i.e., accumulated precipitation, accumulated surface shortwave radiation, monthly air temperature, and model simulated TWS), and the target variable is estimated from GRACE JPL-M observations (207 months in total; April 2002–May 2020 except the gap period of July 2017–May 2018). Other details of the machine learning technique are the same as those developed for TWS projection up to 2060, shown in the Methods.

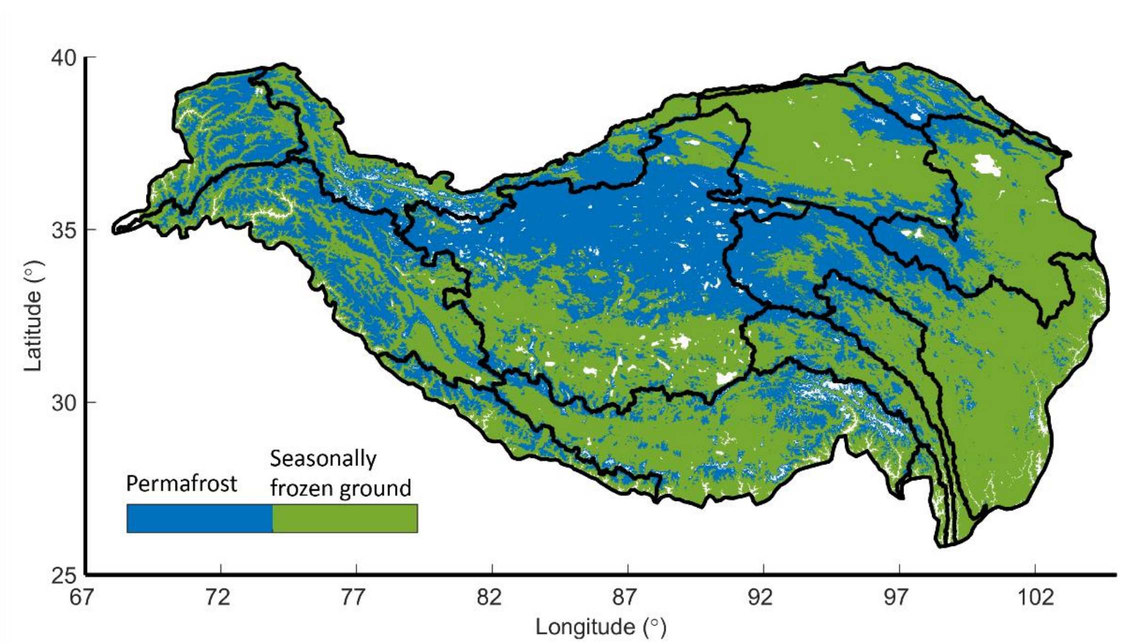

Fig. S6 Spatial distributions of permafrost and seasonally frozen ground over the Tibetan Plateau. Data for generating this figure were provided by Zheng et al. [7]. Permafrost is shown in blue, whereas seasonally frozen ground is shown in green.

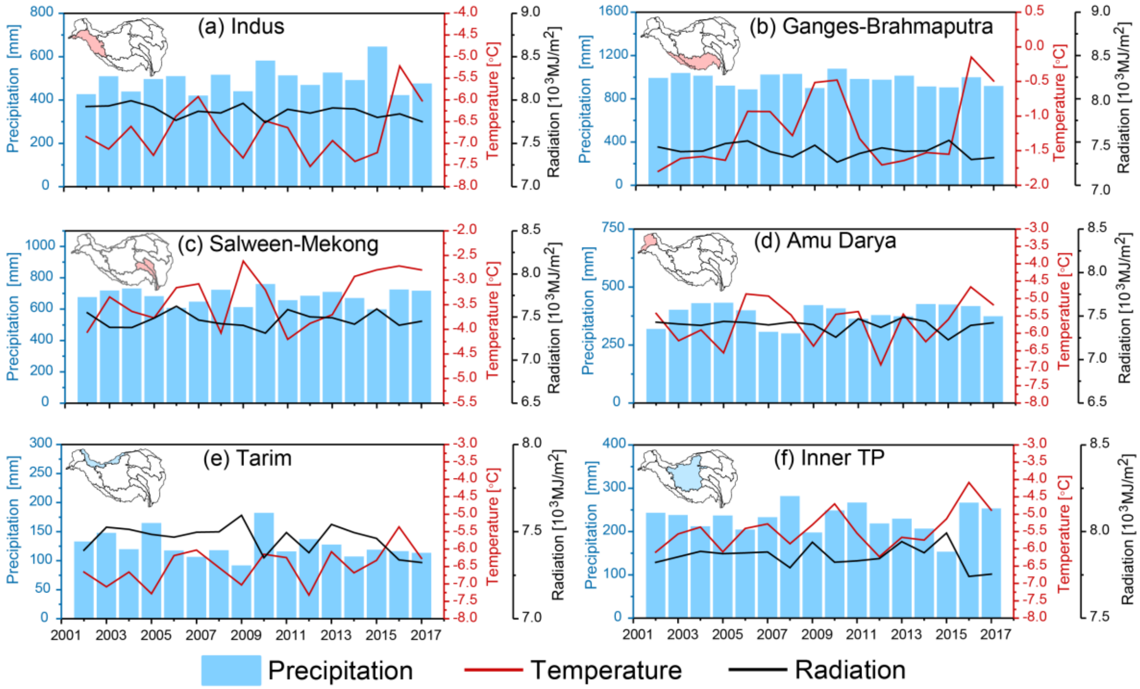

Fig. S7 Annual variations in climate drivers of key basins during 2002–2017. Annual precipitation (light blue bars) is shown on the left y-axis, whereas annual average 2-m temperature (red lines) and annual surface shortwave radiation (black lines) are shown on the right y-axis. Shadow regions of the inserted Tibetan Plateau boundary on the top-left corner denote geographical locations of each river basin, including the **(a)** Indus, **(b)** Ganges-Brahmaputra, **(c)** Salween-Mekong, **(d)** Amy Darya, **(e)** Tarim, and **(f)** Inner TP basins. Red shadows represent regions showing decreases in TWS and blue shadows represent regions showing increases in TWS.

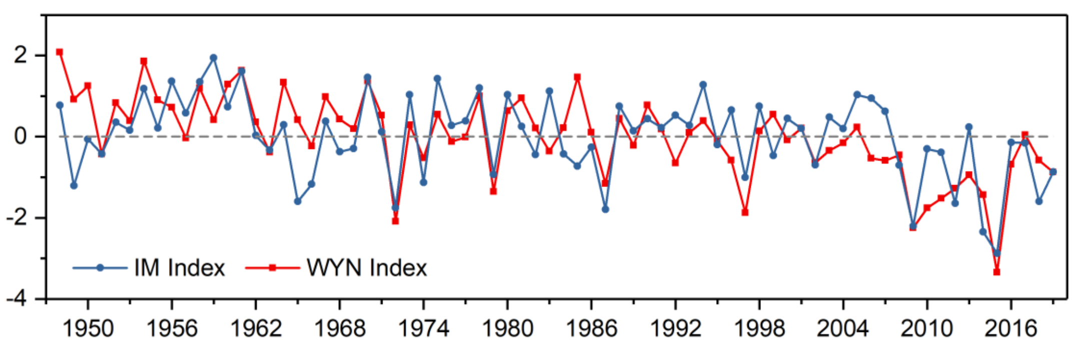

Fig. S8 Variations in monsoon indices during 1948–2019. The blue line shows the Indian Summer Monsoon Index (IM Index), whereas the red line shows the Webster and Yang Monsoon Index (WYM Index) during summer (June–August). Both indices were calculated using NCEP/NCAR Reanalysis data and normalized during 1948–2019, provided by the Asia-Pacific Data-research Center. *Note*: IM Index = U850 (40E–80E, 5N–15N) – U850 (70E–90E, 20N–30N); WYM Index = U850 (40E–110E, EQ–20N) – U200 (40E–110E, EQ–20N).

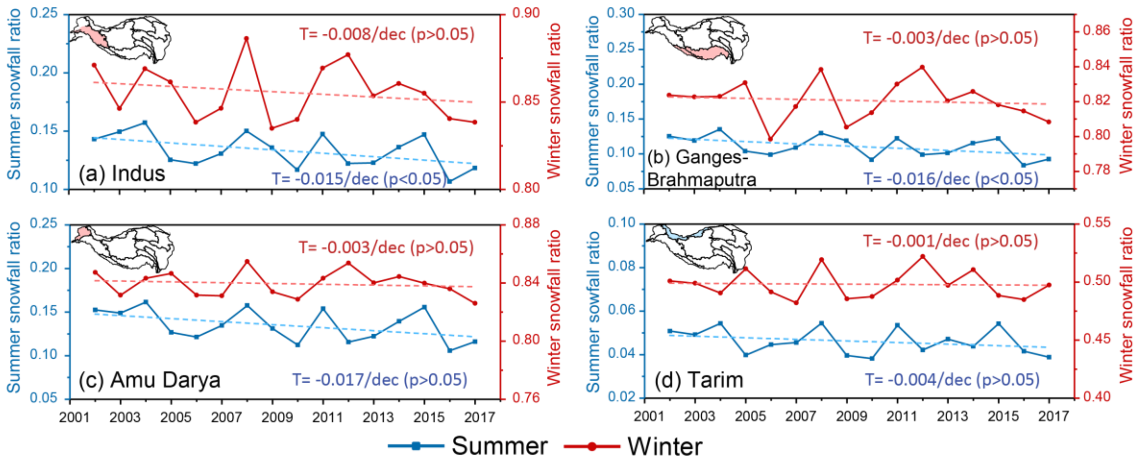

Fig. S9 Snowfall ratios in summer and winter months during 2002–2017. (a) Indus, **(b)** Ganges-Brahmaputra, **(c)** Amu Darya, and **(d)** Tarim basins are analyzed here. The summer snowfall ratio (June–August, solid blue lines) is shown on the left y-axis, whereas the winter snowfall ratio (December–February, solid red lines) is shown on the right y-axis. Dash lines are linear regression trends. Shadow regions of the inserted Tibetan Plateau boundary on the top-left corner denote geographical locations of each river basin, where red shadows denote regions having decreases in TWS and blue shadows denote regions having increases in TWS.

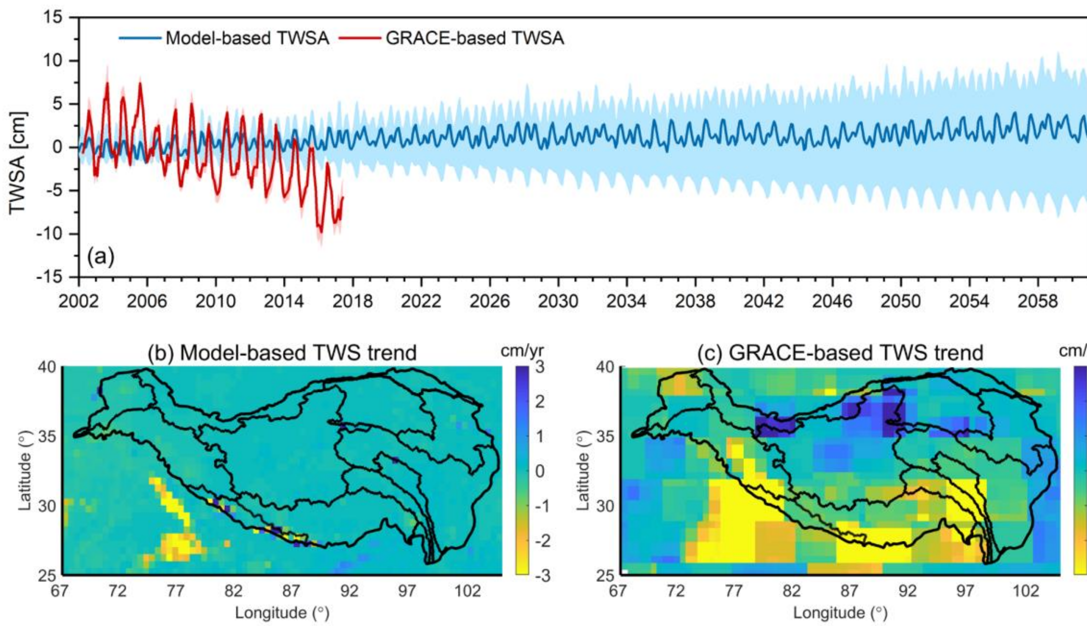

Fig. S10 TWS changes over the Tibetan Plateau from global model simulations. (a) Time series of region-mean TWS anomaly (TWSA) over the Tibetan Plateau. The solid red line shows the mean of four GRACE solutions (JPL-M, CSR-M, JPL-SH, and CSR-SH), and the solid blue line shows the ensemble mean of 23 hydrologic or vegetation models (Table S8) under the mid-range scenario (RCP6.0). Shadows represent ±1 standard deviation among different GRACE solutions or model outputs. **(b–c)** Spatial patterns of TWS trends over the Tibetan Plateau during 2002–2017, estimated by **(b)** the ensemble mean of 23 models and **(c)** GRACE JPL-M solution. All model results are anomalies relative to the 2004–2009 time-mean baseline for comparison with GRACE results.

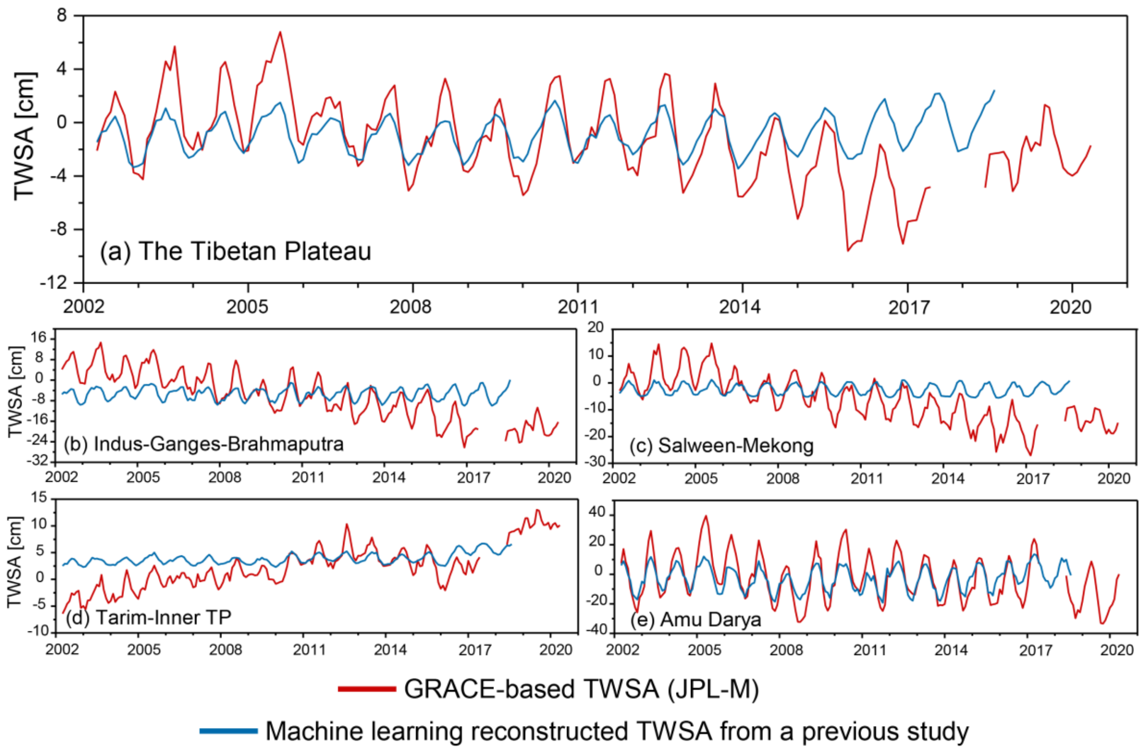

Fig. S11 Reconstructed TWS anomaly (TWSA) from a previous study. Data for generating this figure were provided by Sun et al.[4]. Region-averaged TWSA estimated from GRACE JPL-M is shown as the red line, whereas the reconstructed result is shown as the blue line over the **(a)** Tibetan Plateau, **(b)** Indus-Ganges-Brahmaputra, **(c)** Salween-Mekong, **(d)** Tarim-Inner TP, and **(e)**Amu Darya basin.

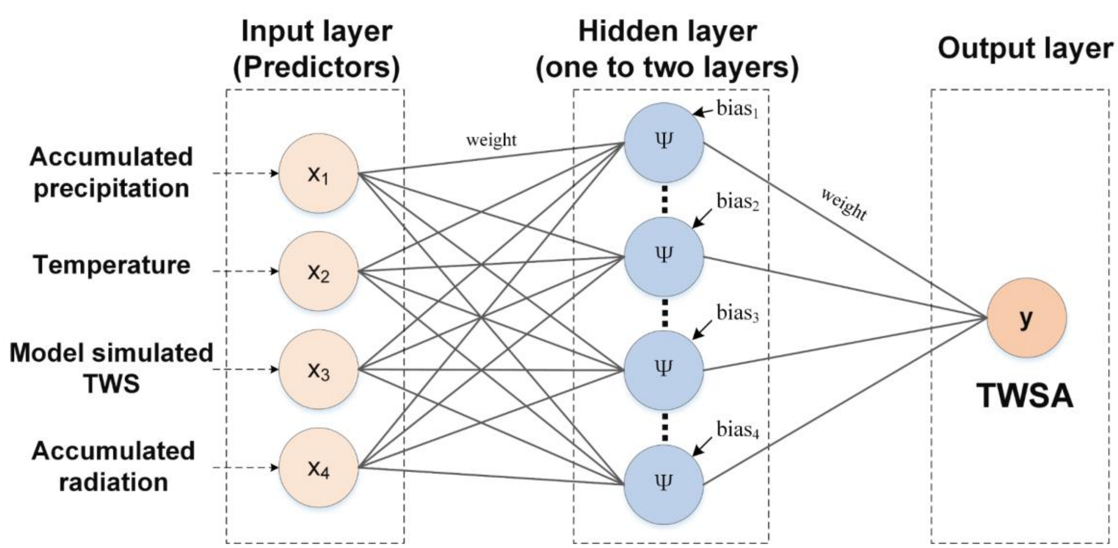

Fig. S12 Structure of the developed artificial neural network in this study.

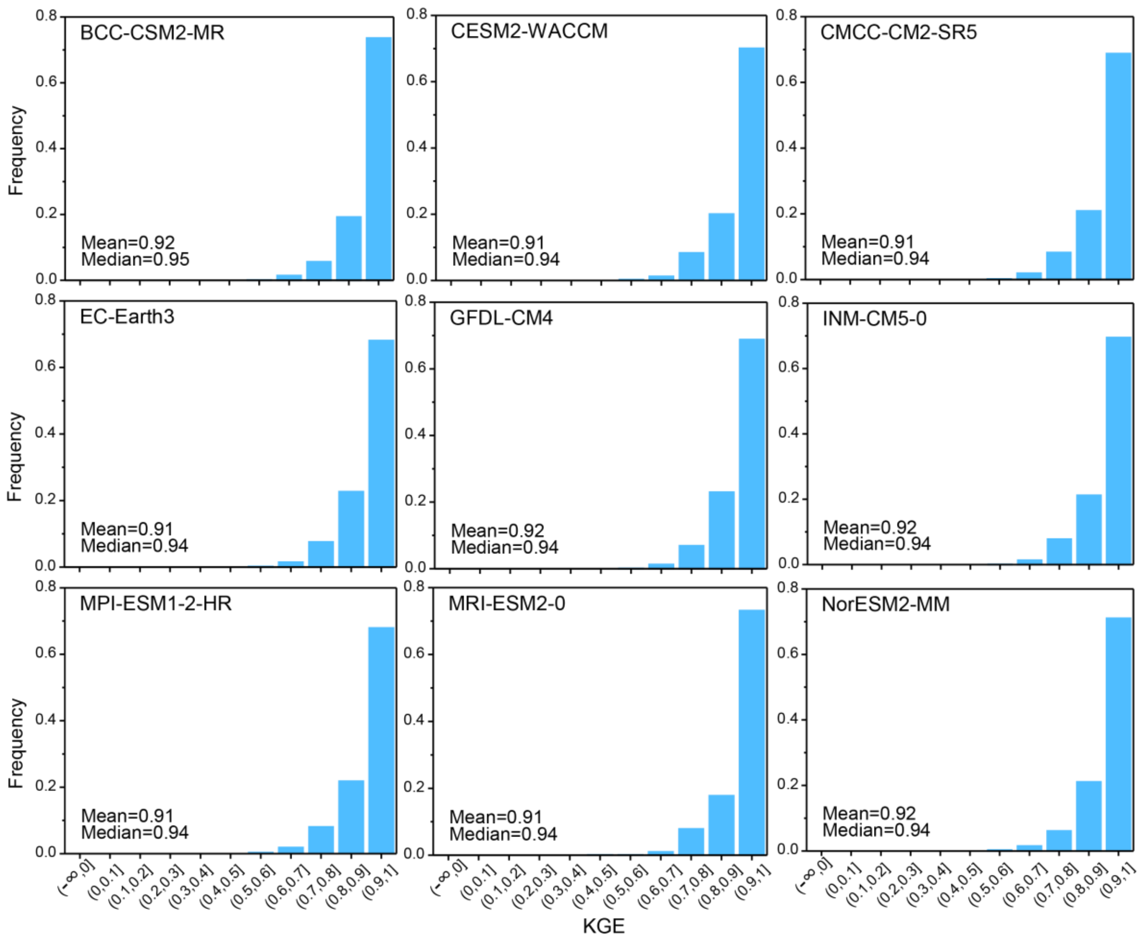

Fig. S13 Histograms of frequency distributions of grid-cell KGE values over the Tibetan Plateau. Outputs in the testing sets (~15% samples) from machine learning models of this study are shown for each CMIP6 forcing separately.

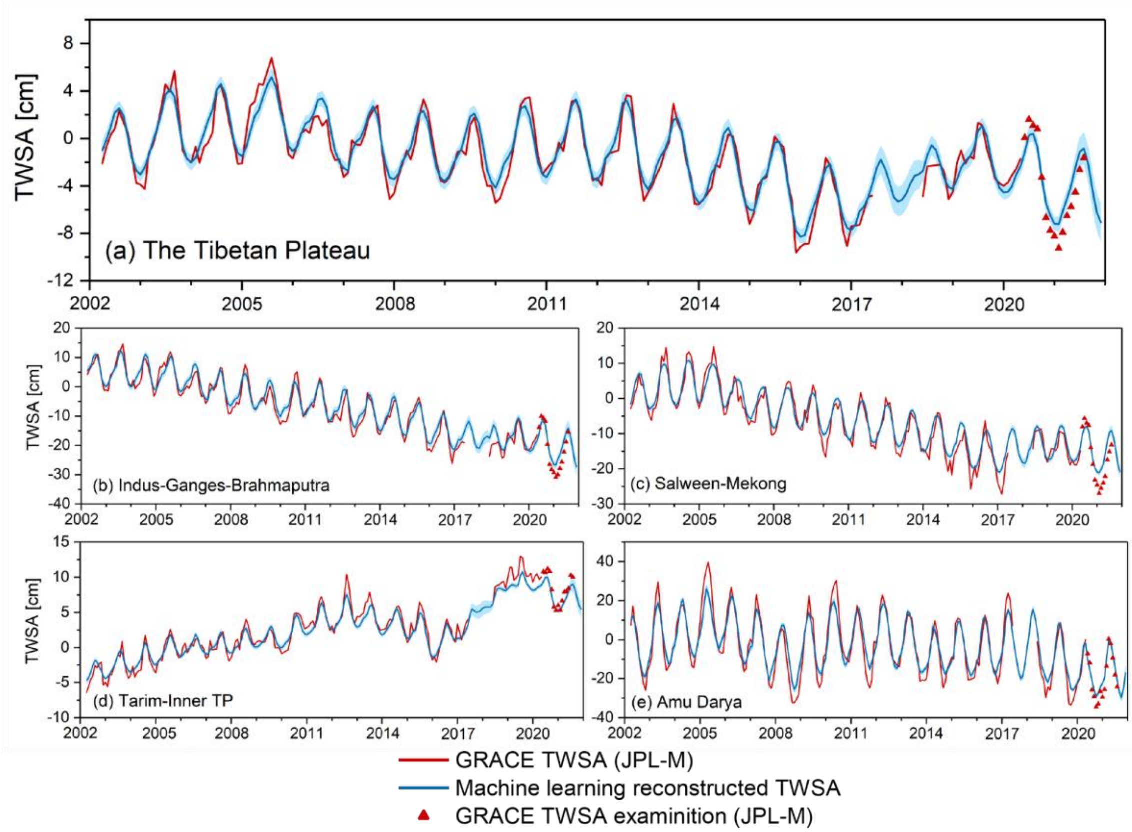

Fig. S14 Reconstructed TWS anomaly (TWSA) during the gap period between GRACE and GRACE-FO. Region-averaged TWSA estimated from GRACE JPL-M and machine learning reconstructed outputs during the 2002–2021 period is presented over the **(a)** Tibetan Plateau, **(b)** Indus-Ganges-Brahmaputra, **(c)** Salween-Mekong, **(d)** Tarim-Inner TP, and **(e)** Amu Darya basins. Red lines show GRACE observations, whereas blue lines show the ensemble mean of reconstructed TWSA from nine CMIP6 forcings. Shadows represent uncertainty range of ±1 standard deviation among outputs from different CMIP6 models. Red dots show GRACE-FO observations during the June 2020–Aug 2021 period that were excluded from training, validating, and testing the machine learning models.

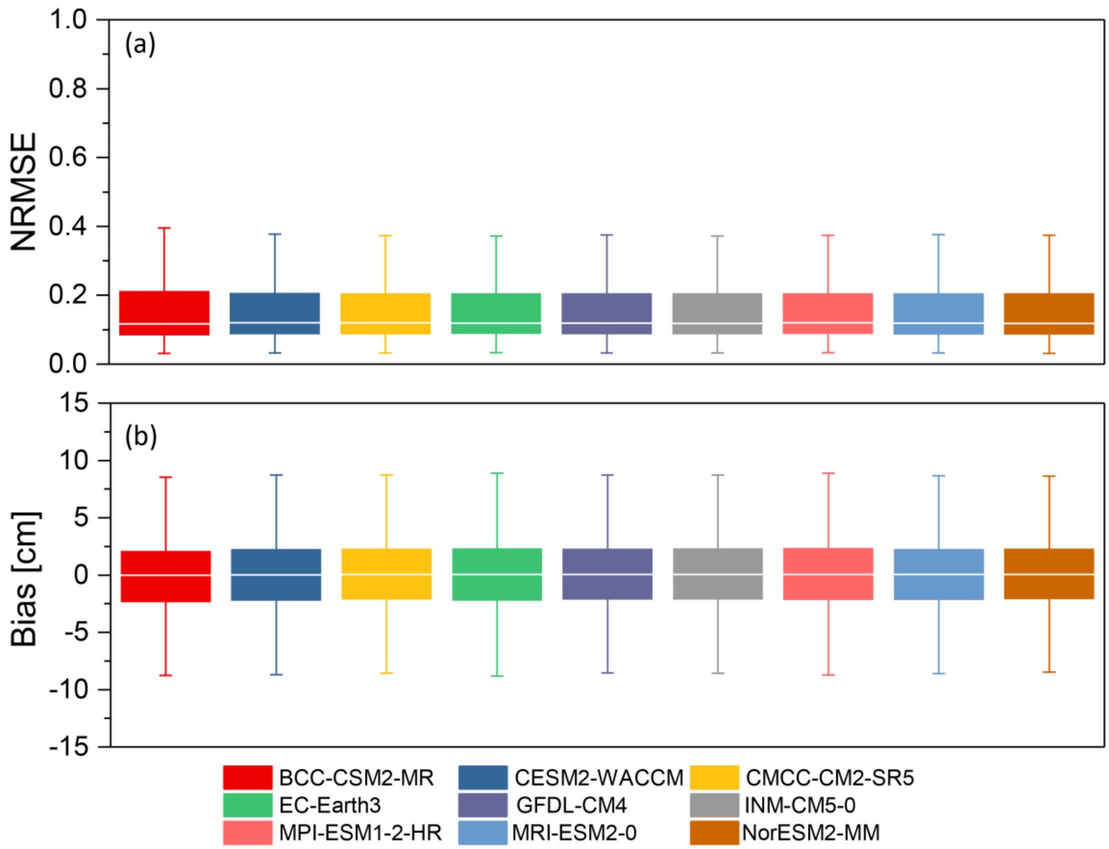

Fig. S15 Boxplots of normalized root mean square error and bias of machine learning output in the testing sets.

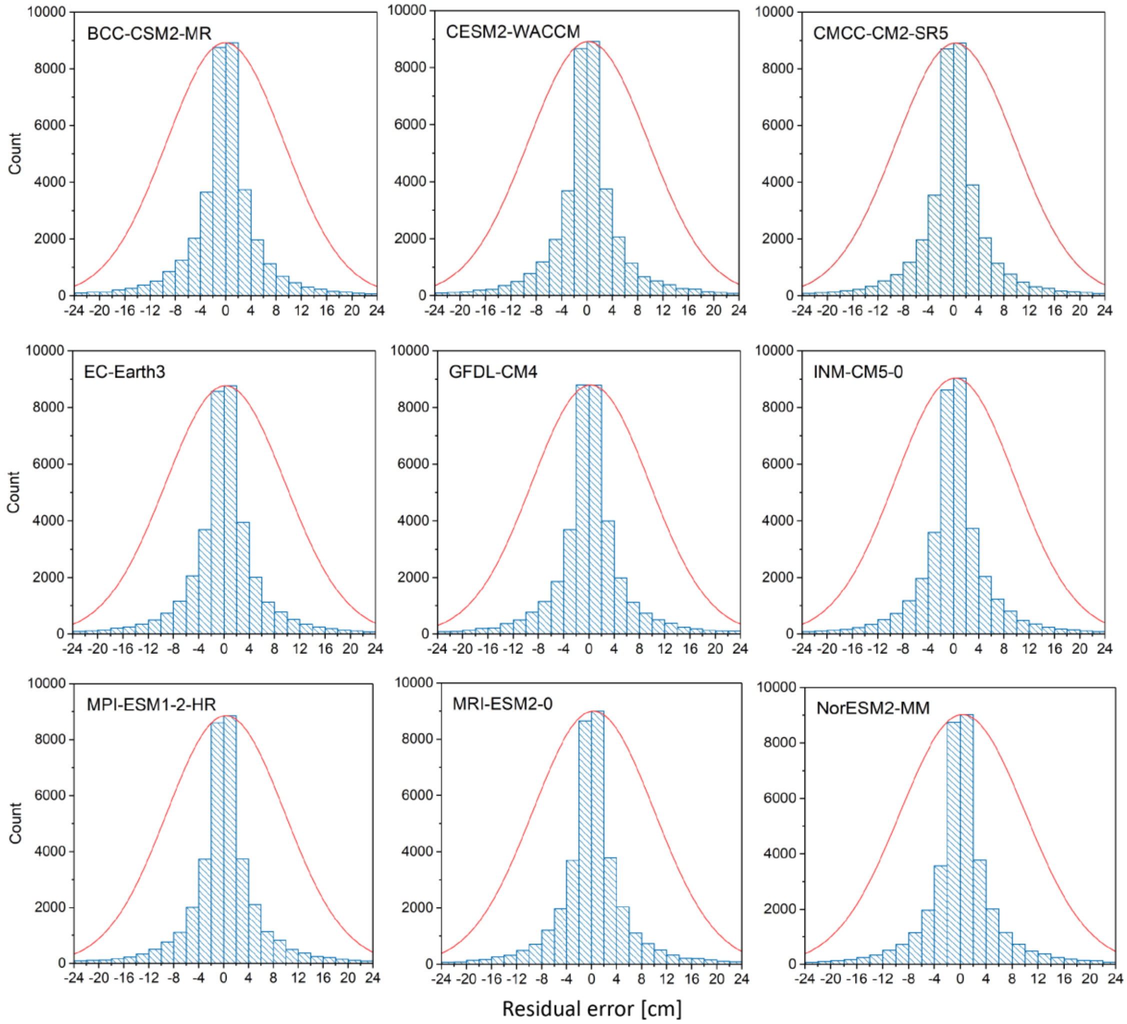

Fig. S16 Histograms and fitted curves of error distribution of machine learning output in the testing sets.

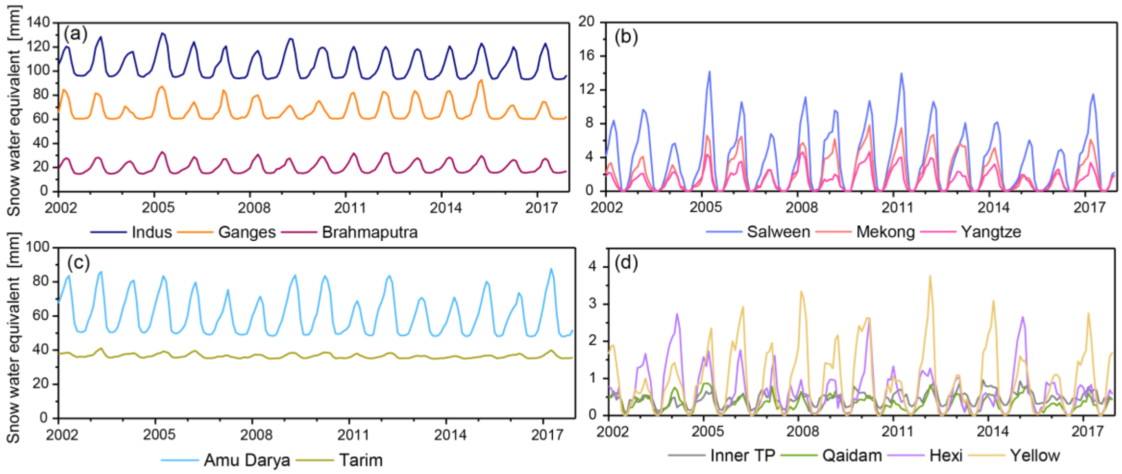

Fig. S17 Variations of snow water equivalent in each basin during 2002–2017. Basin-averaged estimates were derived from the reanalysis ERA5.

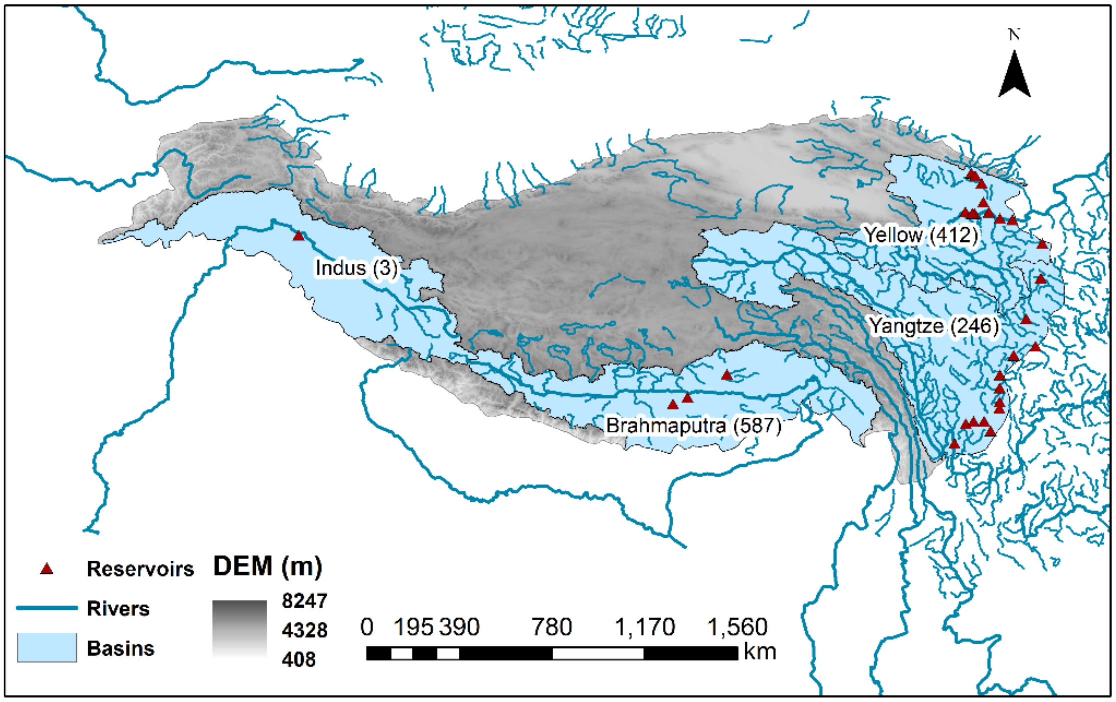

Fig. S18 Reservoirs across the Tibetan Plateau. Basins where reservoirs are distributed are shown in blue, including the Indus, Brahmaputra, Yangtze, and Yellow basins. Values in brackets represent total reservoir areas in each basin, with the unit of km^2.

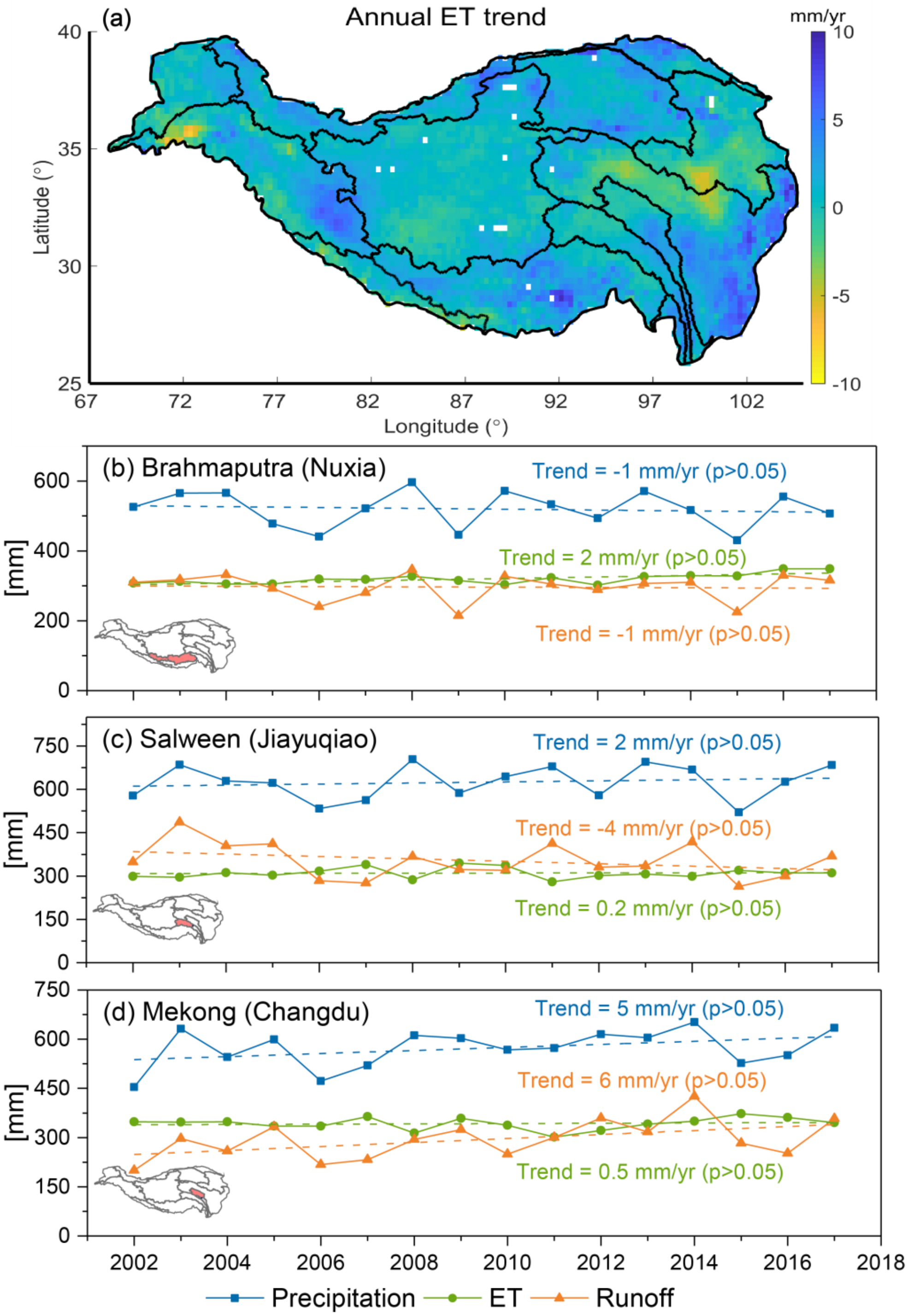

Fig. S19 Variations in precipitation, ET, and observed runoff during 2002–2017. (a) Spatial pattern of annual ET trends over the Tibetan Plateau. **(b)–(d)** Basin-averaged annual precipitation, ET, and observed runoff in the **(b)** Brahmaputra, **(c)** Salween, and **(d)** Mekong basins. Shadow regions of the inserted Tibetan Plateau boundary on the bottom-left corner in **(b)–(d)** denote geographical locations of each river basin. Precipitation data were derived from Integrated Multi-satellitE Retrievals for GPM (IMERG) V06, and ET data were derived from Global Land Evaporation Amsterdam Model v3.5a (GLEAM v3.5a). Runoff observations were derived from the Nuxia (Upper Brahmaputra), Jiayuqiao (Upper Salween), and Changdu (Upper Mekong) gauges.

Supplementary Tables

Table S1 Information on endorheic (closed) and exorheic (open) basins. All variables are derived for the drainage basins within the Tibetan Plateau boundary.

Basin Name	Location range	Elevation range (m)	Basin area (km^2)	Percentage of basin area within the TP boundary to the entire basin area (%)	Glacier area (km^2)	Lake area (km^2)
Endorheic (closed) basins						
Amu Darya	68–75°E, 35–40°N	934–6,935	125,809	20	9,561	
Hexi	93–101°E, 38–40°N	1,950–5,610	61,933	35	1,106	622
Inner TP	79–94°E, 30–39°N	2,854–6,317	709,329	100	7,052	32,300
Qaidam	90–99°E, 35–39°N	2,655–6,552	253,434	100	1,445	1,690
Tarim	73–93°E, 35–40°N	1,805–7,390	191,411	21	15,370	
Exorheic (open) basins						
Brahmaputra	82–98°E, 27–31°N	408–8,247	385,973	59	12,755	1,113
Ganges	78–88°E, 27–31°N	547–7,982	85,273	9	5,885	
Indus	68–82°E, 30–37°N	779–7,528	319,695	37	27,073	1,330
Mekong	94–100°E, 26–34°N	1,403–5,983	90,802	12	229	
Salween	91–99°E, 26–33°N	859–6,382	111,102	42	1,245	192
Yangtze	91–105°E, 27–36°N	781–6,317	482,063	25	1,636	203
Yellow	96–104°E, 32–38°N	1,762–6,090	249,876	29	143	5,688

Table S2 Multisource data sets used for estimating water storages and climate drivers. The time span in this table refers to the period for the data sets used in this study.

Variable	Product name/ data accessibility	Spatial resolution	Temporal resolution	Time span
Estimation for surface, subsurface, and terrestrial water storage				
Terrestrial water storage	GRACE JPL-M	0.5°×0.5°	Monthly	Apr 2002–Jun 2017 and Jun 2018–May 2020
	GRACE CSR-M	0.25°×0.25°		
	GRACE JPL-SH	1°×1°		
	GRACE CSR-SH	1°×1°		
Glacier water storage	Brun et al. [33]	30 m×30 m	Multi-year average	2000–2016
Lake water storage	Li et al. [34]	30 m for lake areas	Monthly	2002–2017
	Wang et al. [39]	30 m for lake areas	Annual	2002–2017
Subsurface water storage	NOAH	0.25°×0.25°	Monthly	2002–2017
	VIC	1°×1°	Monthly	2002–2017
	CLSM	0.25°×0.25°	Daily	2003–2017
Climate drivers				
Precipitation	IMERG	0.1°×0.1°	Daily	2002–2020
2m temperature	ERA5	0.1°×0.1°	Daily	2002–2020
Surface shortwave radiation	ERA5	0.1°×0.1°	Daily	2002–2020

Table S3 Information on CMIP6 models used for future projections.

Model	Institution	Country/ Region	Nominal resolution	lat × lon	Variant label	Data node
BCC-CSM2-MR	BCC	China	100 km	160×320	r1i1p1f1	cmip.bcc.cma.cn
CESM2-WACCM	NCAR	USA	100 km	192×288	r1i1p1f1	esgf-data.ucar.edu
CMCC-CM2-SR5	CMCC	Italy	100 km	192×288	r1i1p1f1	esgf-node2.cmcc.it
EC-Earth3	EC-Earth-Consortium	Europe	100 km	256×512	r1i1p1f1	esg-dn1.nsc.liu.se
GFDL-CM4	NOAA-GFDL	USA	100 km	180×288	r1i1p1f1	esgdata.gfdl.noaa.gov
INM-CM5-0	INM	Russia	100 km	120×180	r1i1p1f1	esgf3.dkrz.de
MPI-ESM1-2-HR	DKRZ	Germany	100 km	192×384	r1i1p1f1	esgf3.dkrz.de
MRI-ESM2-0	MRI	Japan	100 km	160×320	r1i1p1f1	esgf-data2.diasjp.net
NorESM2-MM	NCC	Norway	100 km	192×288	r1i1p1f1	noresg.nird.sigma2.no

Table S4 Water storage changes from the bottom-up approach for each basin during 2002–2017. Except basin area, all components are in the unit of Gt/yr (=km^3 of water/yr). Changes in surface water storage are partitioned into changes in glacier and lake storage, estimated from multisource remote sensing. Changes in subsurface storage were estimated from the ensemble mean of three land surface models.

Name	Area (km^2)	Glacier	Lake	Surface	Subsurface	Total
Amu Darya	125,809	-0.94		-0.94	-0.12	-1.07
Ganges-Brahmaputra	471,246	-7.14	-0.18	-7.33	-2.90	-10.23
Hexi	61,933	-0.17	0.15	-0.03	0.10	0.08
Indus	319,695	-4.07	-0.03	-4.10	-0.42	-4.52
Inner TP	709,329	-0.41	7.36	6.95	-1.58	5.37
Qaidam	253,434	-0.14	0.09	-0.05	0.11	0.06
Salween-Mekong	201,904	-0.68	-0.20	-0.88	-1.20	-2.07
Tarim	191,411	1.09		1.09	0.28	1.37
Yangtze	482,063	-0.32		-0.32	-1.05	-1.37
Yellow	249,876		0.55	0.55	0.17	0.72

Table S5 Agreement in bottom-up and top-down derived TWS changes during 2002–2017. The bottom-up TWS change (shown in bold) is partitioned into changes in surface and subsurface water storage (underlined), where surface water storage changes were estimated by summing up changes in glacier and lake storage. The top-down TWS change (shown in italics) consists of GRACE observations derived from JPL-M, CSR-M, CSR-SH, and JPL-SH, where the top-down GRACE output having the highest agreement with the bottom-up TWS change is shown in red for each study region.

Name	Area (km^2)	**Bottom-Up water storage changes (Gt/yr)**					*Top-Down TWS changes (Gt/yr)*			
		Glacier	Lake	Surface	Subsurface	**Total**	*JPL-M*	*CSR-M*	*JPL-SH*	*CSR-SH*
Amu Darya	125,809	-0.94		-0.94	-0.12	**-1.07**	*-0.70*	*-0.52*	*-0.51*	*-0.53*
Ganges-Brahmaputra	471,246	-7.14	-0.18	-7.33	-2.90	**-10.23**	*-8.39*	*-8.32*	*-7.12*	*-7.02*
Indus	319,695	-4.07	-0.03	-4.10	-0.42	**-4.52**	*-4.83*	*-1.68*	*-2.97*	*-3.06*
Inner TP	709,329	-0.41	7.36	6.95	-1.58	**5.37**	*4.22*	*1.97*	*-0.74*	*-0.79*
Salween-Mekong	201,904	-0.68	-0.20	-0.88	-1.20	**-2.07**	*-3.17*	*-1.70*	*-1.66*	*-1.65*
Tarim	191,411	1.09		1.09	0.28	**1.37**	*1.12*	*0.09*	*0.12*	*0.10*
IGB region (Indus-Ganges-Brahmaputra)	790,941	-11.21	-0.21	-11.42	-3.33	**-14.75**	*-13.22*	*-10.00*	*-10.09*	*-10.08*
Tarim-Inner TP	900,740	0.68	7.36	8.04	-1.30	**6.74**	*5.33*	*2.06*	*-0.63*	*-0.69*
Endorheic TP basins	1,341,916	-0.58	7.60	7.02	-1.21	**5.81**	*5.62*	*2.46*	*-0.31*	*-0.30*
Exorheic TP basins	1,724,785	-12.21	0.14	-12.08	-5.40	**-17.48**	*-15.82*	*-11.92*	*-13.27*	*-13.30*

Table S6 Apportioned water storage changes in each study region during 2002–2017. Except the region area, all components are in the unit of Gt/yr (=km^3 of water/yr). Changes in each storage component were apportioned by multiplying the percentage of its contribution to bottom-up TWS changes by top-down TWS changes estimated from JPL-M. This table is to estimate contributions from glaciers, lakes, and subsurface water storage to TWS trends.

Name	Area (km^2)	Glacier	Lake	Surface	Subsurface	Total
Amu Darya	125,809	-0.62		-0.62	-0.08	-0.70
Ganges-Brahmaputra	471,246	-5.86	-0.15	-6.01	-2.38	-8.39
Indus	319,695	-4.35	-0.03	-4.38	-0.45	-4.83
Inner TP	709,329	-0.32	5.78	5.45	-1.24	4.22
Salween-Mekong	201,904	-1.04	-0.31	-1.34	-1.83	-3.17
Tarim	191,411	0.89		0.89	0.23	1.12
IGB region (Indus-Ganges-Brahmaputra)	790,941	-10.05	-0.19	-10.24	-2.98	-13.22
TI region (Tarim-Inner TP)	900,740	0.54	5.82	6.36	-1.03	5.33
Endorheic TP basins	1,341,916	-0.56	7.34	6.78	-1.17	5.62
Exorheic TP basins	1,724,785	-11.06	0.12	-10.93	-4.89	-15.82

Table S7 Water supply capacity and water demand in key Asian basins during the early and mid-21st century.

	Amu Darya	Indus	Ganges-Brahmaputra	Salween-Mekong	Yangtze	Yellow
Mean annual supply capacity / water demand during the early 21st century (2002–2030)						
TWSA	-82	-156	-127	-133	-18	15
NSC_u	134	179	392	221	138	48
NSC_d	48	154	724	562	455	7
Irrigation demand	134	399	192	43	132	88
Industrial demand	16	8	7	2	10	13
Domestic demand	5	10	26	2	15	8
D	155	417	225	47	156	110
Mean annual supply capacity / water demand during the mid-21st century (2031–2060)						
TWSA	-266	-486	-267	-264	-56	24
NSC_u	124	167	408	230	156	50
NSC_d	43	150	735	604	460	3
Irrigation demand	128	364	166	44	122	80
Industrial demand	24	9	9	3	16	23
Domestic demand	8	18	50	4	22	13
D	161	391	225	51	160	116

Note: TWSA has the unit of mm and all other variables have the unite of mm/yr (basin average). TWSA = terrestrial water storage anomaly; NSC_u = upstream natural supply capacity; NSC_d = downstream natural supply capacity; D = downstream total water demand. All of water demand (irrigation, industrial, and domestic demand) was estimated for downstream basin mean.

Table S8 A summary of global models used for comparison with results of this study.

Model	Prediction forcing	Model Type
CWatM	GFDL-ESM2M / HADGEM2-ES IPSL-CM5A-LR / MIROC5	Global hydrologic model
H08	GFDL-ESM2M / HADGEM2-ES IPSL-CM5A-LR / MIROC5	Global hydrologic model
LPJmL	GFDL-ESM2M / HADGEM2-ES IPSL-CM5A-LR / MIROC5	Dynamic global vegetation model
MPI-HM	GFDL-ESM2M IPSL-CM5A-LR / MIROC5	Global hydrologic model
PCR-GLOBWB	GFDL-ESM2M / HADGEM2-ES IPSL-CM5A-LR / MIROC5	Global hydrologic model
WaterGAP2	GFDL-ESM2M / HADGEM2-ES IPSL-CM5A-LR / MIROC5	Global hydrologic model

Supplementary References:

1. Zhao L, Hu G, Zou D, Wu X, Ma L, Sun Z, *et al.* Permafrost changes and its effects on hydrological processes on Qinghai-Tibet Plateau. *Bulletin of the Chinese Academy of Sciences* 2019, **34**(11)**:** 1233-1246.

2. Yao T, Thompson L, Yang W, Yu W, Gao Y, Guo X, *et al.* Different glacier status with atmospheric circulations in Tibetan Plateau and surroundings. *Nature Climate Change* 2012, **2**(9)**:** 663-667.

3. Zhang G, Ran Y, Wan W, Luo W, Chen W, Xu F, *et al.* 100 years of lake evolution over the Qinghai-Tibet Plateau. *Earth System Science Data* 2021, **13**(8)**:** 3951-3966.

4. Huss M, Hock R. Global-scale hydrological response to future glacier mass loss. *Nature Climate Change* 2018, **8**(2)**:** 135-140.

5. Biemans H, Siderius C, Lutz A, Nepal S, Ahmad B, Hassan T, *et al.* Importance of snow and glacier meltwater for agriculture on the Indo-Gangetic Plain. *Nature Sustainability* 2019, **2**(7)**:** 594-601.

6. Gao J, Yao T, Masson-Delmotte V, Steen-Larsen HC, Wang W. Collapsing glaciers threaten Asia's water supplies. *Nature* 2019, **565**(7737)**:** 19-21.

7. Zheng G, Yang Y, Yang D, Dafflon B, Yi Y, Zhang S, *et al.* Remote sensing spatiotemporal patterns of frozen soil and the environmental controls over the Tibetan Plateau during 2002-2016. *Remote Sensing of Environment* 2020, **247:** 111927.

8. Scanlon BR, Zhang Z, Save H, Sun AY, Mueller Schmied H, van Beek LPH, *et al.* Global models underestimate large decadal declining and rising water storage trends relative to GRACE satellite data. *Proceedings of the National Academy of Sciences of the United States of America* 2018, **115**(6)**:** E1080-E1089.

9. Immerzeel WW, Lutz AF, Andrade M, Bahl A, Biemans H, Bolch T, *et al.* Importance and vulnerability of the world's water towers. *Nature* 2020, **577**(7790)**:** 364-369.

10. Liu B, Li L, Du Yu E, Liang T, Duan S, Hou F, *et al.* Causes of the outburst of Zonag Lake in Hoh Xil,Tibetan Plateau, and its impact on surrounding environment. *Journal of Glaciology and Geocryology* 2016, **38**(2)**:** 305-311.

11. Yao X, Liu S, Sun M, Guo W, Zhang X. Changes of Kusai Lake in Hoh Xil Region and causes of its water overflowing. *Acta Geographica Sinica* 2012, **67**(5)**:** 689-698.

12. Farinotti D, Immerzeel WW, de Kok RJ, Quincey DJ, Dehecq A. Manifestations and mechanisms of the Karakoram glacier Anomaly. *Nature Geoscience* 2020, **13**(1)**:** 8-16.

13. Bao W, Liu S, Wei J, Guo W. Glacier changes during the past 40 years in the West Kunlun Shan. *Journal of Mountain Science* 2015, **12**(2)**:** 344-357.

14. Qin Y, Abatzoglou JT, Siebert S, Huning LS, AghaKouchak A, Mankin JS, *et al.* Agricultural risks from changing snowmelt. *Nature Climate Change* 2020, **10**(5)**:** 459-465.

15. Wang J, Song C, Reager JT, Yao F, Famiglietti JS, Sheng Y, *et al.* Recent global decline in endorheic basin water storages. *Nature Geoscience* 2018, **11**(12)**:** 926-932.

16. Hewitt K. Glacier change, concentration, and elevation effects in the Karakoram Himalaya, Upper Indus Basin. *Mountain Research and Development* 2011, **31**(3)**:** 188-200.

17. Wang B, Fan Z. Choice of south Asian summer monsoon indices. *Bulletin of the American Meteorological Society* 1999, **80**(4)**:** 629-638.

18. Webster PJ, Yang S. Monsoon and ENSO-selectively interactive systems. *Quarterly Journal of the Royal Meteorological Society* 1992, **118**(507)**:** 877-926.

19. Fan F, Mann ME, Lee S, Evans JL. Future changes in the South Asian Summer Monsoon: an analysis of the CMIP3 multimodel projections. *Journal of Climate* 2012, **25**(11)**:** 3909-3928.

20. Tan J, Huffman GJ, Bolvin DT, Nelkin EJ. IMERG V06: Changes to the Morphing Algorithm. *Journal of Atmospheric and Oceanic Technology* 2019, **36**(12)**:** 2471-2482.

21. Hersbach H, Bell B, Berrisford P, Hirahara S, Horanyi A, Munoz-Sabater J, *et al.* The ERA5 global reanalysis. *Quarterly Journal of the Royal Meteorological Society* 2020, **146**(730)**:** 1999-2049.

22. Mihalcea C, Mayer C, Diolaiuti G, Lambrecht A, Smiraglia C, Tartari G. Ice ablation and meteorolopical conditions on the debris-covered area of Baltoro glacier, Karakoram, Pakistan. In: MosleyThompson E, Thompson LG (eds). *Annals of Glaciology, Vol 43, 2006*, vol. 43, 2006, pp 292-300.

23. Bonekamp PNJ, de Kok RJ, Collier E, Immerzeel WW. Contrasting meteorological drivers of the glacier mass balance between the Karakoram and Central Himalaya. *Frontiers in Earth Science* 2019, **7:** 107.

24. de Kok RJ, Tuinenburg OA, Bonekamp PNJ, Immerzeel WW. Irrigation as a potential driver for anomalous glacier behavior in High Mountain Asia. *Geophysical Research Letters* 2018, **45**(4)**:** 2047-2054.

25. Sun Z, Long D, Yang W, Li X, Pan Y. Reconstruction of GRACE data on changes in total water storage over the global land surface and 60 basins. *Water Resources Research* 2020, **56**(4)**:** e2019WR026250.

26. Mo S, Zhong Y, Forootan E, Mehrnegar N, Yin X, Wu J, *et al.* Bayesian convolutional neural networks for predicting the terrestrial water storage anomalies during GRACE and GRACE-FO gap. *Journal of Hydrology* 2022, **604:** 127244.

27. Zhang G, Bolch T, Chen W, Cretaux J-F. Comprehensive estimation of lake volume changes on the Tibetan Plateau during 1976-2019 and basin-wide glacier contribution. *Science of the Total Environment* 2021, **772:** 145463.

28. Rounce DR, Hock R, Shean DE. Glacier mass change in High Mountain Asia through 2100 using the open-source Python Glacier Evolution Model (PyGEM). *Frontiers in Earth Science* 2020, **7:** 331.

29. Li B, Rodell M, Kumar S, Beaudoing HK, Getirana A, Zaitchik BF, *et al.* Global GRACE data assimilation for groundwater and drought monitoring: advances and challenges. *Water Resources Research* 2019, **55**(9)**:** 7564-7586.

30. Liang X, Wood EF, Lettenmaier DP. Modeling ground heat flux in land surface parameterization schemes. *Journal of Geophysical Research-Atmospheres* 1999, **104**(D8)**:** 9581-9600.

31. Koren V, Schaake J, Mitchell K, Duan QY, Chen F, Baker JM. A parameterization of snowpack and frozen ground intended for NCEP weather and climate models. *Journal of Geophysical Research-Atmospheres* 1999, **104**(D16)**:** 19569-19585.

32. Stieglitz M, Ducharne A, Koster R, Suarez M. The impact of detailed snow physics on the simulation of snow cover and subsurface thermodynamics at continental scales. *Journal of Hydrometeorology* 2001, **2**(3)**:** 228-242.

33. Brun F, Berthier E, Wagnon P, Kaab A, Treichler D. A spatially resolved estimate of High Mountain Asia glacier mass balances from 2000 to 2016. *Nature Geoscience* 2017, **10**(9)**:** 668-673.

34. Li X, Long D, Huang Q, Han P, Zhao F, Wada Y. High-temporal-resolution water level and storage change data sets for lakes on the Tibetan Plateau during 2000-2017 using multiple altimetric missions and Landsat-derived lake shoreline positions. *Earth System Science Data* 2019, **11**(4)**:** 1603-1627.

35. Fisher JB, Melton F, Middleton E, Hain C, Anderson M, Allen R, *et al.* The future of evapotranspiration: Global requirements for ecosystem functioning, carbon and climate feedbacks, agricultural management, and water resources. *Water Resources Research* 2017, **53**(4)**:** 2618-2626.

36. Long D, Longuevergne L, Scanlon BR. Uncertainty in evapotranspiration from land surface modeling, remote sensing, and GRACE satellites. *Water Resources Research* 2014, **50**(2)**:** 1131-1151.

37. Li X, Long D, Han Z, Scanlon BR, Sun Z, Han P, *et al.* Evapotranspiration estimation for Tibetan Plateau headwaters using conjoint terrestrial and atmospheric water balances and multisource remote sensing. *Water Resources Research* 2019, **55**(11)**:** 8608-8630.

38. Pokhrel Y, Felfelani F, Satoh Y, Boulange J, Burek P, Gaedeke A, *et al.* Global terrestrial water storage and drought severity under climate change. *Nature Climate Change* 2021, **11:** 226-233.

39. Wang J, Wang L, Li M, Zhu L, Li X. Lake area and volume variation data in the endorheic basin of the Tibetan Plateau from 1989 to 2019. *Zenodo*; https://doi.org/10.5281/zenodo.6578862 (2021).